

Improved measurement of the branching fraction of $h_c \rightarrow \gamma\eta'/\eta$ and search for $h_c \rightarrow \gamma\pi^0$

BESIII Collaboration



E-mail: besiii-publications@ihep.ac.cn

ABSTRACT: The processes $h_c \rightarrow \gamma P (P = \eta', \eta, \pi^0)$ are studied with a sample of $(27.12 \pm 0.14) \times 10^8$ $\psi(3686)$ events collected by the BESIII detector at the BEPCII collider. The decay $h_c \rightarrow \gamma\eta$ is observed for the first time with the significance of 9.0σ , and the branching fraction is determined to be $(3.77 \pm 0.55 \pm 0.13 \pm 0.26) \times 10^{-4}$, while $\mathcal{B}(h_c \rightarrow \gamma\eta')$ is measured to be $(1.40 \pm 0.11 \pm 0.04 \pm 0.10) \times 10^{-3}$, where the first uncertainties are statistical, the second systematic, and the third from the branching fraction of $\psi(3686) \rightarrow \pi^0 h_c$. The combination of these results allows for a precise determination of $R_{h_c} = \frac{\mathcal{B}(h_c \rightarrow \gamma\eta)}{\mathcal{B}(h_c \rightarrow \gamma\eta')}$, which is calculated to be $(27.0 \pm 4.4 \pm 1.0)\%$. The results are valuable for gaining a deeper understanding of $\eta - \eta'$ mixing, and its manifestation within quantum chromodynamics. No significant signal is found for the decay $h_c \rightarrow \gamma\pi^0$, and an upper limit is placed on its branching fraction of $\mathcal{B}(h_c \rightarrow \gamma\pi^0) < 5.0 \times 10^{-5}$, at the 90% confidence level.

KEYWORDS: Charmonium, Radiative decay, BESIII

ARXIV EPRINT: [2405.11585](https://arxiv.org/abs/2405.11585)

Contents

1	Introduction	1
2	BESIII detector and Monte Carlo simulation	2
3	Event selection and background analysis	3
4	Fit and numerical results	5
5	Systematic uncertainties	7
6	Summary	10
	The BESIII Collaboration	14

1 Introduction

The study of $\eta - \eta'$ mixing is a powerful laboratory for testing the $U(1)_A$ anomaly [1] and SU(3) breaking [2] in Quantum Chromodynamics (QCD), and also probes the gluonic content of the $\eta^{(\prime)}$ mesons. Assuming that the light quarks are massless, the η' meson is a pure flavor singlet. Due to flavor-symmetry breaking, there is mixing among the neutral mesons. Without the $U(1)_A$ anomaly, the two iso-singlet mass eigenstates in the pseudoscalar sector would consist of $u\bar{u} + d\bar{d}$ and $s\bar{s}$, respectively. With the $U(1)_A$ anomaly present, these states mix, resulting in the nearly flavor octet or singlet combinations that correspond to the physical η and η' mesons, respectively. This mixing has attracted a great deal of experimental and theoretical interest. From the experimental side, the $\eta - \eta'$ mixing can be studied through the radiative decays of charmonia to η and η' . Recent measurements have mostly focused on the decay of S-wave charmonium states, such as $J/\psi(\psi(3686)) \rightarrow \gamma\eta$ and $\gamma\eta'$ [3, 4]. From the theoretical side, most of the predictions concerned with this topic regarding branching fractions are compatible with experimental data [5]. However, the $\eta - \eta'$ mixing angle extracted from $J/\psi \rightarrow \gamma\eta$ and $\gamma\eta'$ decays, are not consistent among the different theoretical approaches [6–9]. These discrepancies indicate that our understanding of $\eta - \eta'$ mixing is not complete, and that further experimental and theoretical investigations are necessary.

The P -wave singlet charmonium state, h_c , possesses spin-parity quantum numbers that differ from those of the J/ψ . This distinction leads to different characteristics and behavior in its radiative decays and other processes, compared to those of the vector-meson state. The gluonic contributions of $\eta^{(\prime)}$ are significantly suppressed in the radiative decays of the J/ψ [7]. However, in the radiative decays of h_c , this suppression effect is absent. Therefore, the radiative decays of the h_c provide additional insights and information for understanding

of the gluonic contribution of the $\eta^{(\prime)}$ mesons. The h_c radiative decays, $h_c \rightarrow \gamma\eta'$ and $h_c \rightarrow \gamma\eta$, have been investigated at BESIII through the decay $\psi(3686) \rightarrow \pi^0 h_c$. The statistical significances obtained for $h_c \rightarrow \gamma\eta'$ and $h_c \rightarrow \gamma\eta$ are 8.4σ and 4.0σ , respectively [10]. These results have stimulated extensive theoretical discussion [11–14]. The $\eta - \eta'$ mixing angle, associated with the ratio $R_{h_c} = \mathcal{B}(h_c \rightarrow \gamma\eta)/\mathcal{B}(h_c \rightarrow \gamma\eta')$, is determined to be $\phi = 33.8^\circ \pm 2.5^\circ$ through a perturbative QCD calculation [14]. This value is compatible with recent lattice QCD calculations [9, 15], but deviates from other calculations [6, 8]. Since the uncertainty of the mixing angle ϕ is dominated by R_{h_c} , a more precise measurement of this ratio is essential.

Knowledge of the properties of the h_c is poor relative to that of other hidden charmonium states, e.g. the J/ψ . According to the Particle Data Group (PDG) [16], excluding the E1 decay $h_c \rightarrow \gamma\eta_c$, which has a branching fraction of $57 \pm 5\%$, the sum of the branching fractions of known h_c decay modes is only about 3%. Studies of the radiative decays $h_c \rightarrow \gamma P (P = \eta', \eta, \pi^0)$ are particularly desirable as these will provide more direct information on non-perturbative effects in heavy quarkonia [11]. Previous measurements of the branching fractions of $h_c \rightarrow \gamma\eta^{(\prime)}$ have limited precision [10], as listed in TABLE 1, and the decay $h_c \rightarrow \gamma\pi^0$ remains unobserved.

In this paper, we present the improved measurements of the branching fractions of $h_c \rightarrow \gamma\eta^{(\prime)}$ and a search for $h_c \rightarrow \gamma\pi^0$ via $\psi(3686) \rightarrow \pi^0 h_c$, based on $(27.12 \pm 0.14) \times 10^8$ $\psi(3686)$ events [17, 18] collected by the BESIII detector [19], which is about 6 times more than previously collected [17].

2 BESIII detector and Monte Carlo simulation

The BESIII detector [19] records symmetric e^+e^- collisions provided by the BEPCII storage ring [20] in the center-of-mass energy range from 2.0 to 4.95 GeV, with a peak luminosity of $1 \times 10^{33} \text{ cm}^{-2}\text{s}^{-1}$ achieved at $\sqrt{s} = 3.77$ GeV. BESIII has collected large data samples in this energy region [21]. The cylindrical core of the BESIII detector covers 93% of the full solid angle and consists of a helium-based multilayer drift chamber (MDC), a plastic scintillator time-of-flight system (TOF), and a CsI(Tl) electromagnetic calorimeter (EMC), which are all enclosed in a superconducting solenoidal magnet providing a 1.0 T magnetic field. The solenoid is supported by an octagonal flux-return yoke with resistive plate counter muon identification modules interleaved with steel. The charged-particle momentum resolution at 1 GeV/c is 0.5%, and the dE/dx resolution is 6% for electrons from Bhabha scattering. The EMC measures photon energies with a resolution of 2.5% (5%) at 1 GeV in the barrel (end-cap) region. The time resolution in the TOF barrel region is 68 ps, while that in the end-cap region was 110 ps. The end cap TOF system was upgraded in 2015 using multigap resistive plate chamber technology, providing a time resolution of 60 ps [22].

Simulated data samples produced with a GEANT4-based [23] Monte Carlo (MC) package, which includes the geometric description of the BESIII detector and the detector response, are used to determine the detection efficiency and to estimate the background contributions. The simulation includes the beam-energy spread and initial-state radiation (ISR) in e^+e^- annihilations modeled with the generator KKMC [24]. The inclusive MC

sample includes the production of the $\psi(3686)$ resonance, the ISR production of the J/ψ , and the continuum processes incorporated in KKMC [24]. All particle decays are modeled with EVTGEN [25] using branching fractions either taken from PDG [16], when available, or otherwise estimated with LUNDCHARM [26]. Final-state radiation from charged final state particles is incorporated using the PHOTOS package [27].

The signal MC samples for the decay $\psi(3686) \rightarrow \pi^0 h_c$, $h_c \rightarrow \gamma \eta'(\eta, \pi^0)$ are generated by EVTGEN [25]. The decay $\eta' \rightarrow \gamma \pi^+ \pi^-$ is simulated using the DIY model [28], which takes $\rho - \omega$ interference and the box anomaly into account. The decay $\eta' \rightarrow \eta \pi^+ \pi^-$ is generated using the Dalitz distribution of this decay [29] with the subsequent decay of $\eta \rightarrow \gamma \gamma$ produced by a phase-space model. The η directly from h_c decay is reconstructed via both $\eta \rightarrow \gamma \gamma$ and $\eta \rightarrow \pi^+ \pi^- \pi^0$, in which the latter is generated using the Dalitz distribution as measured in Ref. [30]. The $\pi^0 \rightarrow \gamma \gamma$ decay is also generated using the phase-space model.

3 Event section and background analysis

Charged tracks detected in the MDC are required to be within a polar-angle (θ) range of ($|\cos \theta| < 0.93$), where θ is defined with respect to the z axis, which is the symmetry axis of the MDC. The distance of the closest approach to the interaction point (IP) must be less than 10 cm along the z -axis, V_z , and less than 1 cm in the transverse plane, V_{xy} . Photon candidates are identified using showers in the EMC. The deposited energy of each shower must be more than 25 MeV in the barrel region ($|\cos \theta| < 0.80$) and more than 50 MeV in the end-cap region ($0.86 < |\cos \theta| < 0.92$). To exclude showers that originate from charged tracks, the angle subtended by the EMC shower and the position of the closest charged track at the EMC must be greater than 10 degrees as measured from the IP. To suppress electronic noise and showers unrelated to the event, the difference between the EMC time and the event start time is required to be within [0, 700] ns. If there is no charged particle in the final state, e.g. $h_c \rightarrow \gamma \eta$, $\eta \rightarrow \gamma \gamma$, the timing information from EMC cluster is required to be within $|T - T_{\max}| \leq 500$ ns, where T is the time associated with the EMC cluster for each photon candidate, and T_{\max} is the time of the EMC cluster associated with the most energetic photon.

For the decay $\psi(3686) \rightarrow \pi^0 h_c$ with $h_c \rightarrow \gamma \eta'(\eta' \rightarrow \pi^+ \pi^- \eta)$ or $h_c \rightarrow \gamma \eta(\eta \rightarrow \pi^+ \pi^- \pi^0)$, the final states for both processes consist of a $\pi^+ \pi^-$ pair and five photons. Candidate events are required to have two charged tracks with zero net charge and at least five photons. In the event pre-selection, the π^0 mass window is set to be [0.10, 0.16] GeV/ c^2 , and the η from the η' decay is reconstructed by the $\gamma \gamma$ final state within a mass window of [0.45, 0.59] GeV/ c^2 . To reduce contamination and improve the mass resolution, a six-constraint (6C) kinematic fit is performed, which comprises a four-constraint (4C) fit with two additional mass constraints. The 4C fit requires the total four-momentum of charged tracks and photon candidates to be equal to the initial $\psi(3686)$ momentum. In addition, the invariant mass of the $\gamma \gamma$ pair in the decay of $\psi(3686) \rightarrow \pi^0 h_c$ is constrained to the known π^0 mass [16], and the invariant mass of the $\gamma \gamma$ pair from the h_c decay is constrained to the known π^0 or η mass [16], according to the decay chain being analysed.

For the $\psi(3686) \rightarrow \pi^0 h_c$, $h_c \rightarrow \gamma\eta(\eta \rightarrow \pi^+\pi^-\pi^0)$ decay, there are two π^0 candidates in the final state. The higher energy π^0 is taken as the one decaying from the $\psi(3686)$. In the case of multiple candidates in an event, the one with the smallest χ_{6C}^2 value is selected. The χ_{6C}^2 value of $h_c \rightarrow \gamma\eta'(\eta' \rightarrow \pi^+\pi^-\eta)$ or $h_c \rightarrow \gamma\eta(\eta \rightarrow \pi^+\pi^-\pi^0)$ is required to be less than 70 or 40, respectively. To suppress background events with $\gamma\pi^+\pi^-\eta\pi^0$ final states, such as those arising from the decays $\psi(3686) \rightarrow \gamma\chi_{c2}$, $\chi_{c2} \rightarrow \eta\eta$, one η decays to $\gamma\gamma$, another decays to $\pi^+\pi^-\pi^0$, an additional requirement of $\chi_{6C}^2(\gamma\pi^+\pi^-\pi^0\pi^0) < \chi_{6C}^2(\gamma\pi^+\pi^-\eta\pi^0)$ is imposed for the signal candidates of $h_c \rightarrow \gamma\eta(\eta \rightarrow \pi^+\pi^-\pi^0)$. Here $\chi_{6C}^2(\gamma\pi^+\pi^-\pi^0\pi^0)$ is the χ^2 value of 6C kinematic fit under the hypothesis of $\gamma\pi^+\pi^-\pi^0\pi^0$, while $\chi_{6C}^2(\gamma\pi^+\pi^-\eta\pi^0)$ is the χ^2 value of 6C kinematic fit under the hypothesis of $\gamma\pi^+\pi^-\eta\pi^0$.

For the decay of $h_c \rightarrow \gamma\eta'(\eta' \rightarrow \gamma\pi^+\pi^-)$, candidate events are required to have two charged tracks with zero net charge and at least four photons. A 5C kinematic fit, combining a 4C fit with an additional 1C constraint for the π^0 mass, is applied to the decay chain and used to loop over all possible combinations of photons. The combination with the smallest χ_{5C}^2 value is selected and is required to be less than 40. The highest-energy radiative-photon candidate is assigned as coming from the h_c decay, and the lowest-energy candidate to the η' decay.

In the analysis of the fully neutral final states, $\psi(3686) \rightarrow \pi^0 h_c$, where h_c decays into either $\gamma\eta(\eta \rightarrow \gamma\gamma)$ or $\gamma\pi^0(\pi^0 \rightarrow \gamma\gamma)$, at least five photons are required. For the $h_c \rightarrow \gamma\eta(\eta \rightarrow \gamma\gamma)$ decay, a 5C kinematic fit, combining a 4C fit with an additional 1C constraint for the π^0 mass, is used to select the best candidate with the minimum χ_{5C}^2 value by looping over all possible photon combinations. Additionally, the χ_{5C}^2 value is required to be less than 40. The highest energy photon among the three candidates remaining after excluding those two used to reconstruct the π^0 decay, is taken to be the radiative photon from the h_c decay. When selecting $h_c \rightarrow \gamma\pi^0(\pi^0 \rightarrow \gamma\gamma)$ decays, a 6C kinematic fit is performed, which includes a 4C fit and additional 2C constraints, requiring that the invariant mass of each $\gamma\gamma$ pair equals that of the known π^0 mass. We loop over all possible combinations of photons and select those that give the minimum χ_{6C}^2 value. The higher energy of the two π^0 candidates is selected as the one originating from the h_c decay. The χ_{6C}^2 value is required to be less than 20. The χ^2 requirements for the $h_c \rightarrow \gamma\eta'(\eta)$ selection have been optimized by maximizing the $S/\sqrt{S+B}$ figure of merit, where $S(B)$ is the number of signal (background) events in the signal region from the normalized signal (inclusive) MC sample. As there is no significant signal for the decay $h_c \rightarrow \gamma\pi^0$, the figure of merit in this case is defined as $\epsilon/(3/2 + \sqrt{B})$ [31], where ϵ is the signal efficiency.

The remaining dominant background for the $h_c \rightarrow \gamma\eta$, $\eta \rightarrow \gamma\gamma$ decay arises from a fake photon combined with a real photon, thereby forming a fake η signal. This contamination is suppressed by requiring the ratio $R_E = \frac{|E_{\gamma 1} - E_{\gamma 2}|}{P_\eta} < 0.94$, where $E_{\gamma 1}$ and $E_{\gamma 2}$ are the energies of the two photons from the η candidate decay, and P_η is the momentum of the η candidate in the laboratory frame. For the $h_c \rightarrow \gamma\pi^0$ decay, there are five photons in the signal final states. Four of them come from the two π^0 , and one bachelor photon is from the h_c radiative decay. To suppress this bachelor photon combining with other photons to form fake π^0 signal, we require $M(\gamma\gamma_{\text{low}}) > 0.16 \text{ GeV}/c^2$, where γ is the radiative photon, and γ_{low} is the low-energy photon from π^0 in the decay of $\psi(3686) \rightarrow \pi^0 h_c$. Another source

of background comes from the process $\psi(3686)/e^+e^- \rightarrow \gamma X$ with $X \rightarrow \pi_1^0 \pi_2^0$, where X represents possible intermediate states, π_1^0 and π_2^0 are the π^0 with low energy and high energy, respectively. This contamination is suppressed by requiring the cosine of the angle between π_1^0 and π_2^0 , denoted as $\cos \theta_{\pi_1^0 \pi_2^0}$, to be larger than -0.5 .

4 Fit and numerical results

After the above requirements, the momenta of final states are updated according to the kinematic fit for the further analysis. The distributions of the invariant mass $M(\gamma\pi^+\pi^-\eta)$ or $M(\gamma\gamma\pi^+\pi^-)$ versus the invariant mass $M(\pi^+\pi^-\eta)$ or $M(\gamma\pi^+\pi^-)$ of candidate events in data surviving the selection criteria are shown in Figs. 1 (a, b). Throughout this paper, M denotes the invariant mass of an individual particle combination. Clear h_c signals are observed in the $\gamma\eta'$ final states. The η' signal region is defined as $[0.945, 0.970]$ GeV/c^2 in $M(\pi^+\pi^-\eta)$ and $M(\gamma\pi^+\pi^-)$, while its sideband regions are defined as $[0.900, 0.925]$ and $[0.990, 1.015]$ GeV/c^2 for the two η' decay modes. Figures 1 (c, d) show the one-dimensional projections of $M(\gamma\pi^+\pi^-\eta)$ and $M(\gamma\gamma\pi^+\pi^-)$ for candidate events in the η' signal region. Events from the sideband regions are superimposed, normalized by a 0.5 scale factor. No obvious peaking background is found in the η' sideband regions. Therefore, the background is described by an ARGUS function [32], with the threshold parameter fixed to the kinematic threshold of 3.551 GeV/c^2 , while the other parameters are allowed to float. The signal shape is modeled using a combination of Gaussian kernels, implemented using the RooHistPdf [33]

Similarly, the distributions of $M(\gamma\gamma\gamma)$ or $M(\gamma\pi^+\pi^-\pi^0)$ versus $M(\gamma\gamma)$ or $M(\pi^+\pi^-\pi^0)$ of candidate events in data are shown in Figs. 2(a, b). Significant η and h_c signals are observed. For the $\eta \rightarrow \gamma\gamma$ mode, the η signal region lies within $[0.510, 0.580]$ GeV/c^2 , with its sideband regions defined to be $[0.400, 0.470]$ and $[0.620, 0.690]$ GeV/c^2 . For the $\eta \rightarrow \pi^+\pi^-\pi^0$ mode, the η signal region is defined as $[0.535, 0.560]$ GeV/c^2 , with its η sideband regions defined as $[0.490, 0.515]$ and $[0.580, 0.605]$ GeV/c^2 . Figures 2 (c, d) present the one-dimensional projections of $M(\gamma\gamma\gamma)$ and $M(\gamma\pi^+\pi^-\pi^0)$ for candidate events in the η signal region, with background events from the sideband region superimposed, again normalized by a scale factor of 0.5. As there is no significant peaking background evident in the η sideband regions, we utilize similar signal and background functions to those employed in the $h_c \rightarrow \gamma\eta'$ fits. Figure 3 (left) shows the $M(\gamma\pi^0)$ from data for the process $h_c \rightarrow \gamma\pi^0$, and no significant signal is observed.

The branching fraction of $h_c \rightarrow \gamma P$ ($P = \eta', \eta, \pi^0$) is calculated by

$$\mathcal{B}(h_c \rightarrow \gamma P) = \frac{N^{\text{sig}}}{N^{\text{tot}} \cdot \mathcal{B}(\psi(3686) \rightarrow \pi^0 h_c) \prod_i \mathcal{B}_i \epsilon}, \quad (4.1)$$

where N^{sig} is the signal yield, $\prod_i \mathcal{B}_i$ is the product of the branching fractions of the intermediate decays in the decay chain of interest from the PDG [16], ϵ is the detection efficiency, and N^{tot} is the total number of $\psi(3686)$ events.

For the decay of $h_c \rightarrow \gamma\eta'$, two final states are used to reconstruct the η' meson. A simultaneous unbinned maximum-likelihood fit is performed to determine the branching

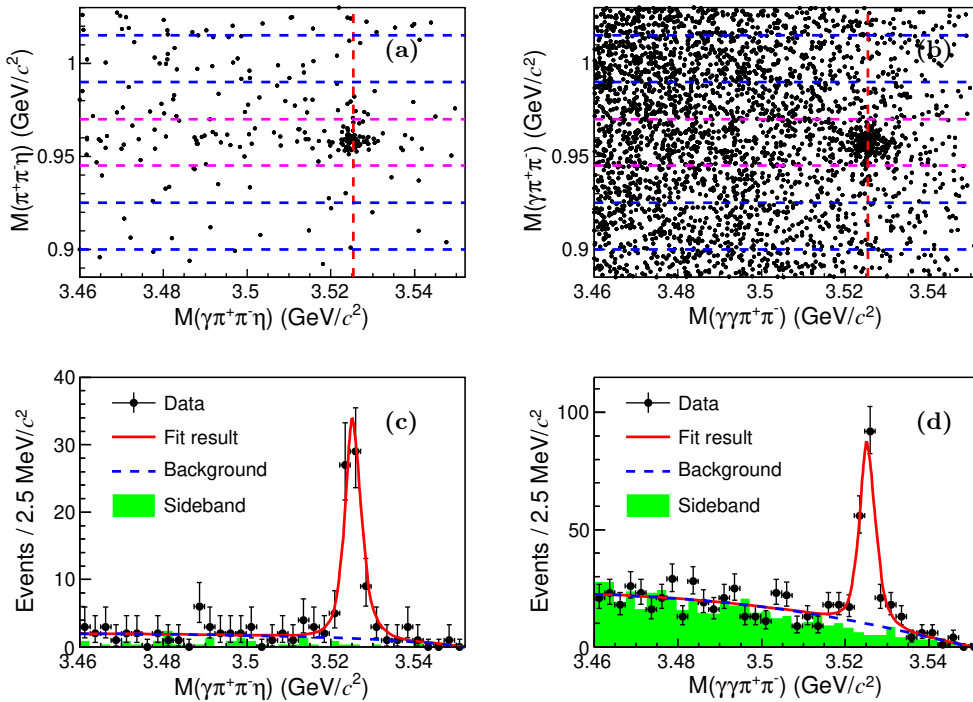


Figure 1. Distributions of (a) $M(\gamma\pi^+\pi^-\eta)$ versus $M(\pi^+\pi^-\eta)$ of the candidates for $h_c \rightarrow \gamma\eta'$ with $\eta' \rightarrow \pi^+\pi^-\eta$, and (b) $M(\gamma\gamma\pi^+\pi^-)$ versus $M(\gamma\pi^+\pi^-)$ of the candidates for $h_c \rightarrow \gamma\eta'$ with $\eta' \rightarrow \gamma\pi^+\pi^-$. The horizontal pink (blue) dashed lines mark the signal (sideband) region(s) of η' and the vertical red dashed lines mark the known h_c mass. (c, d) Simultaneous fit to the $M(\gamma\pi^+\pi^-\eta)$ and $M(\gamma\gamma\pi^+\pi^-)$ distributions.

fraction $\mathcal{B}(h_c \rightarrow \gamma\eta')$, which is taken as a common fit parameter for both η' decay modes. The number of h_c signal events in the two different final states is calculated by

$$N_X^{\text{sig}} = N^{\text{tot}} \cdot \mathcal{B}(\psi(3686) \rightarrow \pi^0 h_c) \cdot \mathcal{B}(\pi^0 \rightarrow \gamma\gamma) \cdot \mathcal{B}(h_c \rightarrow \gamma\eta') \cdot \mathcal{B}(\eta' \rightarrow X) \cdot \epsilon_X, \quad (4.2)$$

where X denotes one of the final states of the η' decay. The projections on $M(\gamma\pi^+\pi^-\eta)$ and $M(\gamma\gamma\pi^+\pi^-)$ of the simultaneous fit are presented in Figs. 1 (c, d).

Similarly, a simultaneous fit is used to extract the branching fraction of $h_c \rightarrow \gamma\eta$, which is treated as a common fit parameter for both η decay modes. The projections on $M(\gamma\gamma\gamma)$ and $M(\gamma\pi^+\pi^-\pi^0)$ of the simultaneous fit are shown in Figs. 2 (c, d). The $h_c \rightarrow \gamma\eta$ signal significance is estimated to be 9.0σ , which is determined by the change of the log-likelihood value and the number of degrees of freedom in the fit with and without the h_c signal. The measured branching fractions for $h_c \rightarrow \gamma\eta'$ and $h_c \rightarrow \gamma\eta$, and their ratio, are listed in TABLE 1.

No significant signal is observed for $h_c \rightarrow \gamma\pi^0$, as can be seen in the left panel of Fig. 3. An upper limit of 5.0×10^{-5} is set on the branching fraction of $h_c \rightarrow \gamma\pi^0$ at the 90% confidence level (C.L.), using a profile likelihood fit, as shown in the right panel of Fig. 3. The green solid line represents the likelihood distribution incorporating additive systematic

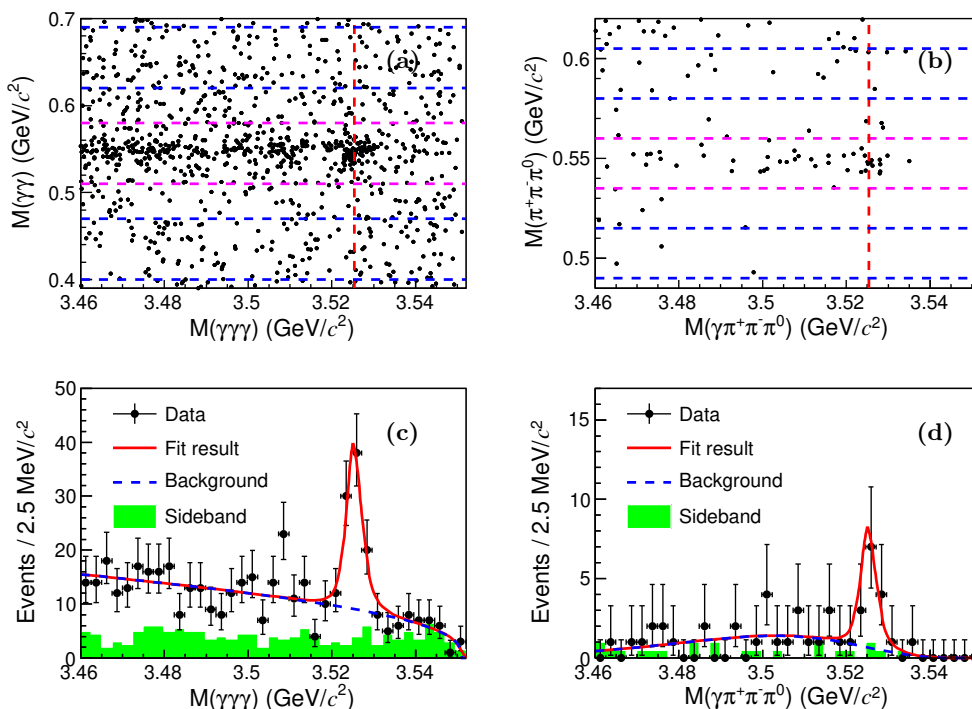


Figure 2. Distributions of (a) $M(\gamma\gamma)$ versus $M(\gamma\gamma)$ of the candidates for $h_c \rightarrow \gamma\eta$ with $\eta \rightarrow \gamma\gamma$, and (b) $M(\gamma\pi^+\pi^-\pi^0)$ versus $M(\pi^+\pi^-\pi^0)$ of the candidates for $h_c \rightarrow \gamma\eta$ with $\eta \rightarrow \pi^+\pi^-\pi^0$. The horizontal pink (blue) dashed lines mark the signal (sideband) region(s) of η and the vertical red dashed lines mark the known h_c mass. (c, d) Simultaneous fit to the $M(\gamma\gamma)$ and $M(\gamma\pi^+\pi^-\pi^0)$ distributions.

	$\mathcal{B}(h_c \rightarrow \gamma\eta')(\times 10^{-3})$	$\mathcal{B}(h_c \rightarrow \gamma\eta)(\times 10^{-4})$	$\mathcal{B}(h_c \rightarrow \gamma\eta)/\mathcal{B}(h_c \rightarrow \gamma\eta')$ (%)
This work	$1.40 \pm 0.11 \pm 0.04 \pm 0.10$	$3.77 \pm 0.55 \pm 0.13 \pm 0.26$	$27.0 \pm 4.4 \pm 1.0$
BESIII [10]	$1.52 \pm 0.27 \pm 0.29$	$4.7 \pm 1.5 \pm 1.4$	$30.7 \pm 11.3 \pm 8.7$

Table 1. Measured branching fractions for $h_c \rightarrow \gamma\eta'$ and $h_c \rightarrow \gamma\eta$, and the ratio of branching fractions for the two decay modes. The first uncertainties are statistical, the second systematic, and the third from the branching fraction of $\psi(3686) \rightarrow \pi^0 h_c$, which cancels and so does not appear in the ratio. Also shown are the previous results from BESIII [10].

uncertainties, while the red dashed line is the convolution of the likelihood curve (green solid line) with multiplicative systematic uncertainties following the method described in Ref [34]. Detailed descriptions of the systematic uncertainties are provided in the subsequent section.

5 Systematic uncertainties

The systematic uncertainties in the measurements of $\mathcal{B}(h_c \rightarrow \gamma\eta'(\eta, \pi^0))$ arise from the understanding of the pion tracking, the photon detection, the π^0 reconstruction, the η mass window, the R ratio requirement for $h_c \rightarrow \gamma\eta$, $\eta \rightarrow \gamma\gamma$, the $\cos\theta_{\pi_1^0\pi_2^0}$ requirement for the

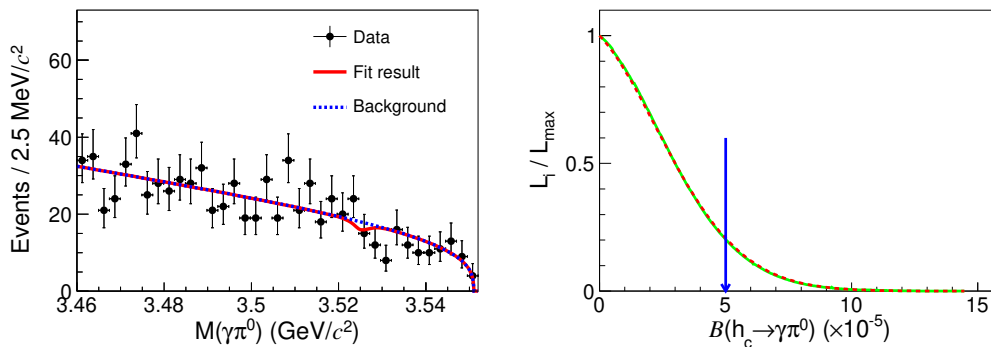


Figure 3. (left) Fit to the $M(\gamma\pi^0)$ distribution of $h_c \rightarrow \gamma\pi^0$ candidates. (right) The green solid line represents the normalized likelihood distribution incorporating additive systematic uncertainties, while the red dashed line corresponds to the aforementioned green solid line with the inclusion of multiplicative systematic uncertainties. The blue arrow indicates the upper limit on the branching fraction at the 90% C.L.

$h_c \rightarrow \gamma\pi^0$ selection, the kinematic fit, the signal shape, the background shape, the assumed branching fractions, and the number of $\psi(3686)$ events, as listed in TABLE 2.

Source	$\eta' \rightarrow \pi^+\pi^-\eta$	$\eta' \rightarrow \pi^+\pi^-\gamma$	$\eta \rightarrow \gamma\gamma$	$\eta \rightarrow \pi^+\pi^-\pi^0$	$\pi^0 \rightarrow \gamma\gamma$
Tracking	2.0	2.0	-	2.0	-
Photon detection	1.5	1.0	1.5	0.5	0.5
π^0 reconstruction	0.5	0.5	0.5	2.4	6.4
η mass window	1.0	-	1.0	-	-
R_E ratio and $\cos\theta_{\pi_1^0\pi_2^0}$	-	-	0.8	-	-
Kinematic fit	0.9	0.6	1.5	1.5	2.8
Signal shape		0.1		0.1	-
Background shape		0.3		2.0	-
$\mathcal{B}_{\eta', \eta, \pi^0}$		1.0		0.4	0.03
$\mathcal{B}(\psi(3686) \rightarrow \pi^0 h_c)$		6.8		6.8	6.8
Number of $\psi(3686)$ events		0.5		0.5	0.5
Sum		7.3		7.5	9.8

Table 2. Relative systematic uncertainties (%) on the branching-fraction measurements, categorised by the decay chain used to reconstruct the final state. A dash (-) indicates that the source is not relevant for that decay.

- *Tracking.* The uncertainty arising from the tracking efficiency is assigned to be 1.0% for each pion from studies of a control sample of $\psi(3686) \rightarrow \pi^+\pi^-J/\psi$, $J/\psi \rightarrow l^+l^-$ decays [35].
- *Photon detection.* The uncertainty in the photon-detection efficiency is studied using a control sample of the $e^+e^- \rightarrow \gamma\mu^+\mu^-$ events. The four-momentum of the initial-state-radiation photon is predicted by the $\mu^+\mu^-$ pair. The photon detection efficiency is defined as the fraction of reconstructed photons with four-momentum matching in the EMC. The systematic uncertainty, defined as the relative difference in efficiency between data and MC simulation, due to photon reconstruction efficiency is observed

always less or equal to 0.5%. Therefore, the conservative systematic uncertainty of 0.5% is assigned to each photon from photon detection efficiency.

- *π^0 reconstruction and η mass window.* The uncertainty of the π^0 reconstruction efficiency is estimated after taking account of its momentum distribution. The relative difference of the π^0 reconstruction efficiencies between data and MC simulation is obtained from a study of $e^+e^- \rightarrow \omega\pi^0$ events at $\sqrt{s} = 3.773$ GeV. This relative difference is found to decrease linearly, $(0.06 - 2.41 \times p)\%$, as a function of momentum p . The associated systematic uncertainties for each decay is listed in TABLE 2. The uncertainty from the η mass window for the $\eta \rightarrow \gamma\gamma$ mode is determined to be 1% per η through the study of a high-purity control sample of $J/\psi \rightarrow p\bar{p}\eta$ events [35].
- *Kinematic fit.* The uncertainty associated with the kinematic fit arises from the charged-track helix parameter correction and the difference in the photon-energy resolution between data and MC simulation. For charged tracks, a correction is made to account for the difference in the distribution of track-helix parameters that is observed between data and MC in a control sample of $J/\psi \rightarrow K^+K^-\pi^+\pi^-$ events [36]. The resolution of the reconstructed photon energy in MC is degraded by 4% to match what is observed in data. The difference between the efficiencies with and without these corrections is taken as the systematic uncertainty.
- *R_E ratio and $\cos\theta_{\pi_1^0\pi_2^0}$.* The systematic uncertainty associated with the R_E ratio ($R_E = |E_{\gamma 1} - E_{\gamma 2}|/P_\eta$) is estimated by an alternative analysis without requiring $R_E < 0.94$, and the difference in the final result is taken as the systematic uncertainty. The uncertainty arising from the $\cos\theta_{\pi_1^0\pi_2^0} > -0.5$ requirement is obtained by varying the cut by ± 0.1 , and taking the maximum deviation observed from the baseline result as the corresponding systematic uncertainty.
- *Signal shape.* The uncertainty associated with the signal shape is estimated by convolving the MC-determined shape with a Gaussian function characterized by free parameters. For the decay of $h_c \rightarrow \gamma\eta$, two Gaussian functions from the signal shapes of $\eta \rightarrow \gamma\gamma$ and $\eta \rightarrow \pi^+\pi^-\pi^0$ share the same parameters due to the low sample size for the $\eta \rightarrow \pi^+\pi^-\pi^0$ mode. For the $h_c \rightarrow \gamma\pi^0$ decay, due to no signal being observed, the Gaussian parameters are fixed to those from the fit to the $h_c \rightarrow \gamma\eta$, $\eta \rightarrow \gamma\gamma$ mass distribution. The difference in the final results is taken as the systematic uncertainty.
- *Background shape.* To assess the uncertainty associated with the description of the background, its shape in the fit is changed from that of the default analysis to be a second-order polynomial function. The difference between the two fit results is assigned as the systematic uncertainty.
- *Input branching fractions.* The uncertainties of the branching fractions are taken from the results reported in the PDG [16].

- *Number of $\psi(3686)$ events.* The total number of $\psi(3686)$ events is determined by using inclusive hadronic decays, as described in Ref. [17]. The uncertainty on the number of $\psi(3686)$ events is estimated to be 0.5%.

The systematic uncertainty on the upper limit of signal events $N_{h_c \rightarrow \gamma \pi^0}^{\text{up}}$ at 90% C.L. includes contributions from both additive and multiplicative sources. The additive sources comprise those from the signal shape, background shape, and $\cos \theta_{\pi_1^0 \pi_2^0} > -0.5$ requirement. Each of them is considered separately, and the upper limit is recomputed. The largest value, which comes from the variation in signal shape, is chosen as the conservative estimation. The other sources listed in TABLE 2 are multiplicative. To include multiplicative systematics, the obtained likelihood curve is used to convolute a Gaussian function in which the uncertainty is taken as a parameter [34]. The likelihood curves before and after consider the uncertainty are shown in the right panel of Fig. 3.

The relative systematic uncertainties in the branching-fraction measurements are summarized in TABLE 2. The systematic uncertainties depend on the η or η' decay modes, in which the uncertainty from the tracking, the photon detection, the π^0 reconstruction, the η mass window, R ratio, and kinematic fit, are combined by a weighted average, considering the number of signal events for each case [38]. The total systematic uncertainty is obtained by summing all contributions in quadrature, assuming they are independent of each other.

6 Summary

We perform the studies of the decays of $h_c \rightarrow \gamma \eta'$, $\gamma \eta$ and $\gamma \pi^0$ via $\psi(3686) \rightarrow \pi^0 h_c$, using $(27.12 \pm 0.14) \times 10^8$ $\psi(3686)$ events collected by the BESIII detector. The decay $h_c \rightarrow \gamma \eta$ is observed for the first time with a statistical significance of 9.0σ and its branching fraction is measured to be $\mathcal{B}(h_c \rightarrow \gamma \eta) = (3.77 \pm 0.55 \pm 0.13 \pm 0.26) \times 10^{-4}$, where the first uncertainty is statistical, the second systematic, and the third arises from the knowledge of the branching fraction of $\psi(3686) \rightarrow \pi^0 h_c$. Additionally, an improved measurement of $\mathcal{B}(h_c \rightarrow \gamma \eta') = (1.40 \pm 0.11 \pm 0.04 \pm 0.10) \times 10^{-3}$ is obtained. From these results, the ratio $R_{h_c} = \frac{\mathcal{B}(h_c \rightarrow \gamma \eta)}{\mathcal{B}(h_c \rightarrow \gamma \eta')}$ is calculated to be $(27.0 \pm 4.4 \pm 1.0)\%$, where the common systematic uncertainties between the two branching fractions are accounted for. These measurement results are consistent with the previous measurements [10], with the improved precision by more than a factor of two. Our result favors the prediction in Ref. [14], suggesting comparable contributions from both the quark-antiquark content and the gluonic content in $\eta^{(\prime)}$. Furthermore, these improved measurements offer valuable prospects for the study of SU(3)-flavor symmetries [2]. We firstly search for $h_c \rightarrow \gamma \pi^0$, no significant signal is found, and an upper limit of $\mathcal{B}(h_c \rightarrow \gamma \pi^0) < 5.0 \times 10^{-5}$ is set on its branching fraction at the 90% C.L.

Acknowledgments

The BESIII Collaboration thanks the staff of BEPCII and the IHEP computing center for their strong support. This work is supported in part by National Key R&D Program

of China under Contracts Nos. 2020YFA0406300, 2020YFA0406400, 2023YFA1606000; National Natural Science Foundation of China (NSFC) under Contracts Nos. 12375070, 12375071, 11635010, 11735014, 11935015, 11935016, 11935018, 12025502, 12035009, 12035013, 12061131003, 12192260, 12192261, 12192262, 12192263, 12192264, 12192265, 12221005, 12225509, 12235017, 12361141819; the Chinese Academy of Sciences (CAS) Large-Scale Scientific Facility Program; the CAS Center for Excellence in Particle Physics (CCEPP); Joint Large-Scale Scientific Facility Funds of the NSFC and CAS under Contract No. U2032108, U1832207; 100 Talents Program of CAS; The Institute of Nuclear and Particle Physics (INPAC) and Shanghai Key Laboratory for Particle Physics and Cosmology; German Research Foundation DFG under Contracts Nos. 455635585, FOR5327, GRK 2149; Istituto Nazionale di Fisica Nucleare, Italy; Knut and Alice Wallenberg Foundation under Contracts Nos. 2021.0174, 2021.0299; Ministry of Development of Turkey under Contract No. DPT2006K-120470; National Research Foundation of Korea under Contract No. NRF-2022R1A2C1092335; National Science and Technology fund of Mongolia; National Science Research and Innovation Fund (NSRF) via the Program Management Unit for Human Resources & Institutional Development, Research and Innovation of Thailand under Contract No. B16F640076; Polish National Science Centre under Contract No. 2019/35/O/ST2/02907; Swedish Research Council under Contract No. 2019.04595; The Swedish Foundation for International Cooperation in Research and Higher Education under Contract No. CH2018-7756; U. S. Department of Energy under Contract No. DE-FG02-05ER41374.

References

- [1] E. Witten, *Current algebra theorems for the U(1) "Goldstone boson"*, *Nucl. Phys. B* **156**, (1979) 269; G. Veneziano, *U(1) without instantons*, *Nucl. Phys. B* **159**, (1979) 213.
- [2] F. J. Gilman and R. Kauffman, *$\eta - \eta'$ mixing angle*, *Phys. Rev. D* **36** (1987) 2761; T. Feldmann, *QUARK STRUCTURE OF PSEUDOSCALAR MESONS*, *Int. J. Mod. Phys. A* **15**, (2000) 159; R. Escribano and E. Royo, *$\pi^0 - \eta - \eta'$ mixing from $V \rightarrow P\gamma$ and $P \rightarrow V\gamma$ decays*, *Phys. Lett. B* **807**, (2020) 135534.
- [3] BESIII Collaboration, *Study of two-photon decays of pseudoscalar mesons via J/ψ radiative decays*, *Phys. Rev. D* **97**, (2018) 072014; BESIII Collaboration, *Measurement of the absolute branching fractions of $J\psi \rightarrow \gamma\eta$ and η decay modes*, *Phys. Rev. D* **104**, (2021), 092004.
- [4] BESIII Collaboration, *Measurement of branching fractions for $\psi(3686) \rightarrow \gamma\eta'$, $\gamma\eta$, and $\gamma\pi^0$* , *Phys. Rev. D* **96**, (2017) 052003.
- [5] V. A. Novikov, M. A. Shifman, A. I. Vainshtein, and V. I. Zakharov, *A theory of the $J/\psi \rightarrow \eta(\eta')\gamma$ decays*, *Nucl. Phys.* **165**, (1980) 55; K.-T. Chao, *Issue of $\psi \rightarrow \gamma\eta$, $\gamma\eta'$ decays and $\eta - \eta'$ mixing*, *Phys. Rev. D* **39**, (1989) 1353; K. T. Chao, *Mixing of η , η' with cc , bb states and their radiative decays*, *Nucl. Phys. B* **335**, (1990) 101; J. M. Gerard and E. Kou, *$\eta - \eta'$ masses and mixing: a large N_c reappraisal* *Phys. Lett. B* **616**, (2005) 85; Y. P. Kuang, Y. P. Yi, and B. Fu, *Multipole expansion in quantum chromodynamics and the radiative decays $J/\psi \rightarrow \gamma + \eta$ and $J/\psi \rightarrow \gamma + \pi^0$* , *Phys. Rev. D* **42**, (1990) 2300.
- [6] T. Feldmann, P. Kroll, and B. Stech, *Mixing and decay constants of pseudoscalar mesons*, *Phys. Rev. D* **58**, (1998) 114006.

- [7] J. K. He and Y. D. Yang, *Revisiting the radiative decays $J/\psi \rightarrow \gamma\eta^{(\prime)}$ in perturbative QCD*, *Nucl. Phys. B* **943**, (2019) 114627.
- [8] ETM Collaboration, *η and η' Mixing from Lattice QCD*, *Phys. Rev. Lett.* **111**, (2013) 181602.
- [9] UKQCD Collaboration, *Study of the η and η' mesons with improved staggered fermions*, *Phys. Rev. D* **86**, (2012) 014504.
- [10] M. Ablikim *et al.* (BESIII Collaboration), *Observation of h_c Radiative Decay $h_c \rightarrow \gamma\eta'$ and Evidence for $h_c \rightarrow \gamma\eta$* , *Phys. Rev. Lett.* **116**, (2016) 251802.
- [11] R. L. Zhu and J. P. Dai, *Radiative $h_{c/b}$ decays to η or η'* , *Phys. Rev. D* **94**,(2016) 094034.
- [12] Q. Wu, G. Li, and Y. W. Zhang, *Study on the radiative decays of h_c via intermediate meson loops model*, *Eur. Phys. J. C* **77**, 336 (2017).
- [13] C. J. Fan and J. K. He, *Radiative decays of h_c to the light mesons $\eta^{(\prime)}$: A perturbative QCD calculation*, *Phys. Rev. D* **100**, (2019) 0344005.
- [14] J. K. He and C. J. Fan, *Revisiting the P-wave charmonium radiative decays $h_c \rightarrow \gamma\eta^{(\prime)}$ with relativistic corrections*, *Phys. Rev. D* **103**, (2021) 114006.
- [15] ETM Collaboration, *Flavor-singlet meson decay constants from $N_f = 2 + 1 + 1$ twisted mass lattice QCD*, *Phys. Rev. D* **97**, (2018) 054508.
- [16] Particle Data Group, *Review of Particle Physics*, *PTEP* **2022** (2022) 083C01.
- [17] BESIII Collaboration, *Determination of the number of $\psi(3686)$ events at BESIII*, *Chin. Phys. C* **42**, (2013) 023001.
- [18] BESIII Collaboration, *Determination of the number of $\psi(3686)$ events taken at BESIII*, [arXiv:2403.06766](https://arxiv.org/abs/2403.06766).
- [19] BESIII Collaboration, *Design and construction of the BESIII detector*, *Nucl. Instrum. Meth. A* **614** (2010) 345.
- [20] C. H. Yu *et al.*, *BEPCII Performance and Beam Dynamics Studies on Luminosity*, Proceedings of IPAC2016, Busan, Korea, 2016, [doi:10.18429/JACoW-IPAC2016-TUYA01](https://doi.org/10.18429/JACoW-IPAC2016-TUYA01).
- [21] BESIII Collaboration, *Future Physics Programme of BESIII*, *Chin. Phys. C* **44**, (2020) 040001; J. Lu, Y. Xiao, X. Ji, *Online monitoring of the center-of-mass energy from real data at BESIII*, *Radiat. Detect. Technol. Methods* **4**, (2020) 337-344.
- [22] X. Li *et al.*, *Study of MRPC technology for BESIII endcap-TOF upgrade*, *Radiat. Detect. Technol. Methods* **1** (2017) 13; Y. X. Guo *et al.*, *The study of time calibration for upgraded end cap TOF of BESIII*, *Radiat. Detect. Technol. Methods* **1** (2017) 15; P. Cao *et al.*, *Design and construction of the new BESIII endcap Time-of-Flight system with MRPC Technology*, *Nucl. Instrum. Meth. A* **953** (2020) 163053.
- [23] GEANT4 Collaboration, *GEANT4—a simulation toolkit*, *Nucl. Instrum. Meth. A* **506** (2003) 250.
- [24] S. Jadach, B. F. L. Ward and Z. Was, *Coherent exclusive exponentiation for precision Monte Carlo calculations*, *Phys. Rev. D* **63** (2001) 113009; *The precision Monte Carlo event generator KK for two-fermion final states in e^+e^- collisions*, *Comput. Phys. Commun.* **130** (2000) 260.
- [25] D. J. Lange, *The EvtGen particle decay simulation package*, *Nucl. Instrum. Meth. A* **462** (2001) 152; R. G. Ping, *Event generators at BESIII*, *Chin. Phys. C* **32** (2008) 599.

- [26] J. C. Chen, G. S. Huang, X. R. Qi, D. H. Zhang and Y. S. Zhu, *Event generator for J/ψ and $\psi(2S)$ decay*, *Phys. Rev. D* **62** (2000) 034003; R. L. Yang, R. G. Ping and H. Chen, *Tuning and Validation of the Lundcharm Model with J/ψ Decays*, *Chin. Phys. Lett.* **31** (2014) 061301.
- [27] E. Richter-Was, *QED bremsstrahlung in semileptonic B and leptonic τ decays*, *Phys. Lett. B* **303** (1993) 163.
- [28] BESIII Collaboration, *Precision Study of $\eta' \rightarrow \gamma\pi^+\pi^-$ Decay Dynamics*, *Phys. Rev. Lett.* **120** (2018) 024003.
- [29] BESIII Collaboration, *Measurement of the matrix elements for the decays $\eta' \rightarrow \eta\pi^+\pi^-$ and $\eta' \rightarrow \eta\pi^0\pi^0$* , *Phys. Rev. D* **97**, (2018) 012003.
- [30] BESIII Collaboration, *Measurement of the matrix elements for the decays $\eta \rightarrow \pi^+\pi^-\pi^0$ and $\eta/\eta' \rightarrow \pi^0\pi^0\pi^0$* , *Phys. Rev. D* **92** (2015) 012014.
- [31] G. Punzi, *Sensitivity of searches for new signals and its optimization*, eConf **C030908**, (2003) MODT002. [[arXiv:physics/0308063](#) [physics]].
- [32] ARGUS Collaboration, *Measurement of the polarization in the decay $B \rightarrow J/\psi K^*$* , *Phys. Lett. B* **340** (1994) 217.
- [33] W. Verkerke and D. P. Kirkby, *The RooFit toolkit for data modeling*, eConf **C0303241**, (2003) MOLT007, [[arXiv:physics/0306116](#) [physics]].
- [34] K. Stenson, *A more exact solution for incorporating multiplicative systematic uncertainties in branching ratio limits*, [arXiv: physics/0605236](#).; X. X.liu, X. R. Lyu, and Y. S. Zhu, *Combined estimation for multi-measurements of branching ratio*, *Chin. Phys. C* **39**, (2015) 103001.
- [35] BESIII Collaboration, *Evidence for ψ' Decays into $\gamma\pi^0$ and $\gamma\eta$* , *Phys. Rev. Lett.* **105** (2010) 261801.
- [36] BESIII Collaboration, *Search for hadronic transition $\chi_{cJ} \rightarrow \eta_c\pi^+\pi^-$ and observation of $\chi_{cJ} \rightarrow K\bar{K}\pi\pi$* , *Phys. Rev. D* **87** (2013) 012002.
- [37] BESIII Collaboration, *Measurements of $h_c(^1P_1)$ in ψ' Decays*, *Phys. Rev. Lett.* **104** (2010) 132002.
- [38] BESIII Collaboration, *Observation of $\chi_{c2} \rightarrow \eta'\eta'$ and $\chi_{c0,2} \rightarrow \eta\eta'$* , *Phys. Rev. D* **96** (2017) 112006.

The BESIII Collaboration

M. Ablikim¹, M. N. Achasov^{4,c}, P. Adlarson⁷⁵, O. Afedulidis³, X. C. Ai⁸⁰, R. Aliberti³⁵, A. Amoroso^{74A,74C}, Q. An^{71,58,a}, Y. Bai⁵⁷, O. Bakina³⁶, I. Balossino^{29A}, Y. Ban^{46,h}, H.-R. Bao⁶³, V. Batzskaya^{1,44}, K. Begzsuren³², N. Berger³⁵, M. Berlowski⁴⁴, M. Bertani^{28A}, D. Bettoni^{29A}, F. Bianchi^{74A,74C}, E. Bianco^{74A,74C}, A. Bortone^{74A,74C}, I. Boyko³⁶, R. A. Briere⁵, A. Brueggemann⁶⁸, H. Cai⁷⁶, X. Cai^{1,58}, A. Calcaterra^{28A}, G. F. Cao^{1,63}, N. Cao^{1,63}, S. A. Cetin^{62A}, J. F. Chang^{1,58}, G. R. Che⁴³, Y. Z. Che^{1,58,63}, G. Chelkov^{36,b}, C. Chen⁴³, C. H. Chen⁹, Chao Chen⁵⁵, G. Chen¹, H. S. Chen^{1,63}, H. Y. Chen²⁰, M. L. Chen^{1,58,63}, S. J. Chen⁴², S. L. Chen⁴⁵, S. M. Chen⁶¹, T. Chen^{1,63}, X. R. Chen^{31,63}, X. T. Chen^{1,63}, Y. B. Chen^{1,58}, Y. Q. Chen³⁴, Z. J. Chen^{25,i}, Z. Y. Chen^{1,63}, S. K. Choi¹⁰, G. Cibinetto^{29A}, F. Cossio^{74C}, J. J. Cui⁵⁰, H. L. Dai^{1,58}, J. P. Dai⁷⁸, A. Dbeyssi¹⁸, R. E. de Boer³, D. Dedovich³⁶, C. Q. Deng⁷², Z. Y. Deng¹, A. Denig³⁵, I. Denysenko³⁶, M. Destefanis^{74A,74C}, F. De Mori^{74A,74C}, B. Ding^{66,1}, X. X. Ding^{46,h}, Y. Ding³⁴, Y. Ding⁴⁰, J. Dong^{1,58}, L. Y. Dong^{1,63}, M. Y. Dong^{1,58,63}, X. Dong⁷⁶, M. C. Du¹, S. X. Du⁸⁰, Y. Y. Duan⁵⁵, Z. H. Duan⁴², P. Egorov^{36,b}, Y. H. Fan⁴⁵, J. Fang⁵⁹, J. Fang^{1,58}, S. S. Fang^{1,63}, W. X. Fang¹, Y. Fang¹, Y. Q. Fang^{1,58}, R. Farinelli^{29A}, L. Fava^{74B,74C}, F. Feldbauer³, G. Felici^{28A}, C. Q. Feng^{71,58}, J. H. Feng⁵⁹, Y. T. Feng^{71,58}, M. Fritsch³, C. D. Fu¹, J. L. Fu⁶³, Y. W. Fu^{1,63}, H. Gao⁶³, X. B. Gao⁴¹, Y. N. Gao^{46,h}, Yang Gao^{71,58}, S. Garbolino^{74C}, I. Garzia^{29A,29B}, L. Ge⁸⁰, P. T. Ge⁷⁶, Z. W. Ge⁴², C. Geng⁵⁹, E. M. Gersabeck⁶⁷, A. Gilman⁶⁹, K. Goetzen¹³, L. Gong⁴⁰, W. X. Gong^{1,58}, W. Gradl³⁵, S. Gramigna^{29A,29B}, M. Greco^{74A,74C}, M. H. Gu^{1,58}, Y. T. Gu¹⁵, C. Y. Guan^{1,63}, A. Q. Guo^{31,63}, L. B. Guo⁴¹, M. J. Guo⁵⁰, R. P. Guo⁴⁹, Y. P. Guo^{12,g}, A. Guskov^{36,b}, J. Gutierrez²⁷, K. L. Han⁶³, T. T. Han¹, F. Hanisch³, X. Q. Hao¹⁹, F. A. Harris⁶⁵, K. K. He⁵⁵, K. L. He^{1,63}, F. H. Heinsius³, C. H. Heinz³⁵, Y. K. Heng^{1,58,63}, C. Herold⁶⁰, T. Holtmann³, P. C. Hong³⁴, G. Y. Hou^{1,63}, X. T. Hou^{1,63}, Y. R. Hou⁶³, Z. L. Hou¹, B. Y. Hu⁵⁹, H. M. Hu^{1,63}, J. F. Hu^{56,j}, S. L. Hu^{12,g}, T. Hu^{1,58,63}, Y. Hu¹, G. S. Huang^{71,58}, K. X. Huang⁵⁹, L. Q. Huang^{31,63}, X. T. Huang⁵⁰, Y. P. Huang¹, Y. S. Huang⁵⁹, T. Hussain⁷³, F. Hölzken³, N. Hüskens³⁵, N. in der Wiesche⁶⁸, J. Jackson²⁷, S. Janchiv³², J. H. Jeong¹⁰, Q. Ji¹, Q. P. Ji¹⁹, W. Ji^{1,63}, X. B. Ji^{1,63}, X. L. Ji^{1,58}, Y. Y. Ji⁵⁰, X. Q. Jia⁵⁰, Z. K. Jia^{71,58}, D. Jiang^{1,63}, H. B. Jiang⁷⁶, P. C. Jiang^{46,h}, S. S. Jiang³⁹, T. J. Jiang¹⁶, X. S. Jiang^{1,58,63}, Y. Jiang⁶³, J. B. Jiao⁵⁰, J. K. Jiao³⁴, Z. Jiao²³, S. Jin⁴², Y. Jin⁶⁶, M. Q. Jing^{1,63}, X. M. Jing⁶³, T. Johansson⁷⁵, S. Kabana³³, N. Kalantar-Nayestanaki⁶⁴, X. L. Kang⁹, X. S. Kang⁴⁰, M. Kavatsyuk⁶⁴, B. C. Ke⁸⁰, V. Khachatryan²⁷, A. Khoukaz⁶⁸, R. Kiuchi¹, O. B. Kolcu^{62A}, B. Kopf³, M. Kuessner³, X. Kui^{1,63}, N. Kumar²⁶, A. Kupsc^{44,75}, W. Kühn³⁷, J. J. Lane⁶⁷, L. Lavezzi^{74A,74C}, T. T. Lei^{71,58}, Z. H. Lei^{71,58}, M. Lellmann³⁵, T. Lenz³⁵, C. Li⁴⁷, C. Li⁴³, C. H. Li³⁹, Cheng Li^{71,58}, D. M. Li⁸⁰, F. Li^{1,58}, G. Li¹, H. B. Li^{1,63}, H. J. Li¹⁹, H. N. Li^{56,j}, Hui Li⁴³, J. R. Li⁶¹, J. S. Li⁵⁹, K. Li¹, K. L. Li¹⁹, L. J. Li^{1,63}, L. K. Li¹, Lei Li⁴⁸, M. H. Li⁴³, P. R. Li^{38,k,l}, Q. M. Li^{1,63}, Q. X. Li⁵⁰, R. Li^{17,31}, S. X. Li¹², T. Li⁵⁰, W. D. Li^{1,63}, W. G. Li^{1,a}, X. Li^{1,63}, X. H. Li^{71,58}, X. L. Li⁵⁰, X. Y. Li^{1,63}, X. Z. Li⁵⁹, Y. G. Li^{46,h}, Z. J. Li⁵⁹, Z. Y. Li⁷⁸, C. Liang⁴², H. Liang^{1,63}, H. Liang^{71,58}, Y. F. Liang⁵⁴, Y. T. Liang^{31,63}, G. R. Liao¹⁴, Y. P. Liao^{1,63}, J. Libby²⁶, A. Limphirat⁶⁰, C. C. Lin⁵⁵, D. X. Lin^{31,63}, T. Lin¹, B. J. Liu¹, B. X. Liu⁷⁶, C. Liu³⁴, C. X. Liu¹, F. Liu¹, F. H. Liu⁵³, Feng Liu⁶, G. M. Liu^{56,j}, H. Liu^{38,k,l}, H. B. Liu¹⁵, H. H. Liu¹, H. M. Liu^{1,63}, Huihui Liu²¹, J. B. Liu^{71,58}, J. Y. Liu^{1,63}, K. Liu^{38,k,l}, K. Y. Liu⁴⁰, Ke Liu²², L. Liu^{71,58}, L. C. Liu⁴³, Lu Liu⁴³, M. H. Liu^{12,g}, P. L. Liu¹, Q. Liu⁶³, S. B. Liu^{71,58}, T. Liu^{12,g}, W. K. Liu⁴³, W. M. Liu^{71,58}, X. Liu^{38,k,l}, X. Liu³⁹, Y. Liu⁸⁰, Y. Liu^{38,k,l}, Y. B. Liu⁴³, Z. A. Liu^{1,58,63}, Z. D. Liu⁹, Z. Q. Liu⁵⁰, X. C. Lou^{1,58,63}, F. X. Lu⁵⁹, H. J. Lu²³, J. G. Lu^{1,58}, X. L. Lu¹, Y. Lu⁷, Y. P. Lu^{1,58}, Z. H. Lu^{1,63}, C. L. Luo⁴¹, J. R. Luo⁵⁹, M. X. Luo⁷⁹, T. Luo^{12,g}, X. L. Luo^{1,58}, X. R. Lyu⁶³, Y. F. Lyu⁴³, F. C. Ma⁴⁰, H. Ma⁷⁸, H. L. Ma¹, J. L. Ma^{1,63}, L. L. Ma⁵⁰, L. R. Ma⁶⁶, M. M. Ma^{1,63}, Q. M. Ma¹, R. Q. Ma^{1,63}, T. Ma^{71,58}, X. T. Ma^{1,63}, X. Y. Ma^{1,58}, Y. M. Ma³¹, F. E. Maas¹⁸, M. Maggiora^{74A,74C}, S. Malde⁶⁹, Y. J. Mao^{46,h}, Z. P. Mao¹, S. Marcello^{74A,74C}, Z. X. Meng⁶⁶, J. G. Messchendorp^{13,64}, G. Mezzadri^{29A}, H. Miao^{1,63},

T. J. Min⁴², R. E. Mitchell²⁷, X. H. Mo^{1,58,63}, B. Moses²⁷, N. Yu. Muchnoi^{4,c}, J. Muskalla³⁵,
 Y. Nefedov³⁶, F. Nerling^{18,e}, L. S. Nie²⁰, I. B. Nikolaev^{4,c}, Z. Ning^{1,58}, S. Nisar^{11,m}, Q. L. Niu^{38,k,l},
 W. D. Niu⁵⁵, Y. Niu⁵⁰, S. L. Olsen⁶³, Q. Ouyang^{1,58,63}, S. Pacetti^{28B,28C}, X. Pan⁵⁵, Y. Pan⁵⁷,
 A. Pathak³⁴, Y. P. Pei^{71,58}, M. Pelizaeus³, H. P. Peng^{71,58}, Y. Y. Peng^{38,k,l}, K. Peters^{13,e},
 J. L. Ping⁴¹, R. G. Ping^{1,63}, S. Plura³⁵, V. Prasad³³, F. Z. Qi¹, H. Qi^{71,58}, H. R. Qi⁶¹, M. Qi⁴²,
 T. Y. Qi^{12,g}, S. Qian^{1,58}, W. B. Qian⁶³, C. F. Qiao⁶³, X. K. Qiao⁸⁰, J. J. Qin⁷², L. Q. Qin¹⁴,
 L. Y. Qin^{71,58}, X. P. Qin^{12,g}, X. S. Qin⁵⁰, Z. H. Qin^{1,58}, J. F. Qiu¹, Z. H. Qu⁷², C. F. Redmer³⁵,
 K. J. Ren³⁹, A. Rivetti^{74C}, M. Rolo^{74C}, G. Rong^{1,63}, Ch. Rosner¹⁸, M. Q. Ruan^{1,58}, S. N. Ruan⁴³,
 N. Salone⁴⁴, A. Sarantsev^{36,d}, Y. Schelhaas³⁵, K. Schoenning⁷⁵, M. Scodreggio^{29A}, K. Y. Shan^{12,g},
 W. Shan²⁴, X. Y. Shan^{71,58}, Z. J. Shang^{38,k,l}, J. F. Shangguan¹⁶, L. G. Shao^{1,63}, M. Shao^{71,58},
 C. P. Shen^{12,g}, H. F. Shen^{1,8}, W. H. Shen⁶³, X. Y. Shen^{1,63}, B. A. Shi⁶³, H. Shi^{71,58}, H. C. Shi^{71,58},
 J. L. Shi^{12,g}, J. Y. Shi¹, Q. Q. Shi⁵⁵, S. Y. Shi⁷², X. Shi^{1,58}, J. J. Song¹⁹, T. Z. Song⁵⁹, W. M. Song^{34,1},
 Y. J. Song^{12,g}, Y. X. Song^{46,h,n}, S. Sosio^{74A,74C}, S. Spataro^{74A,74C}, F. Stieler³⁵, S. S. Su⁴⁰,
 Y. J. Su⁶³, G. B. Sun⁷⁶, G. X. Sun¹, H. Sun⁶³, H. K. Sun¹, J. F. Sun¹⁹, K. Sun⁶¹, L. Sun⁷⁶,
 S. S. Sun^{1,63}, T. Sun^{51,f}, W. Y. Sun³⁴, Y. Sun⁹, Y. J. Sun^{71,58}, Y. Z. Sun¹, Z. Q. Sun^{1,63},
 Z. T. Sun⁵⁰, C. J. Tang⁵⁴, G. Y. Tang¹, J. Tang⁵⁹, M. Tang^{71,58}, Y. A. Tang⁷⁶, L. Y. Tao⁷²,
 Q. T. Tao^{25,i}, M. Tat⁶⁹, J. X. Teng^{71,58}, V. Thoren⁷⁵, W. H. Tian⁵⁹, Y. Tian^{31,63}, Z. F. Tian⁷⁶,
 I. Uman^{62B}, Y. Wan⁵⁵, S. J. Wang⁵⁰, B. Wang¹, B. L. Wang⁶³, Bo Wang^{71,58}, D. Y. Wang^{46,h},
 F. Wang⁷², H. J. Wang^{38,k,l}, J. J. Wang⁷⁶, J. P. Wang⁵⁰, K. Wang^{1,58}, L. L. Wang¹, M. Wang⁵⁰,
 N. Y. Wang⁶³, S. Wang^{12,g}, S. Wang^{38,k,l}, T. Wang^{12,g}, T. J. Wang⁴³, W. Wang⁷², W. Wang⁵⁹,
 W. P. Wang^{35,58,71,o}, X. Wang^{46,h}, X. F. Wang^{38,k,l}, X. J. Wang³⁹, X. L. Wang^{12,g}, X. N. Wang¹,
 Y. Wang⁶¹, Y. D. Wang⁴⁵, Y. F. Wang^{1,58,63}, Y. H. Wang^{38,k,l}, Y. L. Wang¹⁹, Y. N. Wang⁴⁵,
 Y. Q. Wang¹, Yaqian Wang¹⁷, Yi Wang⁶¹, Z. Wang^{1,58}, Z. L. Wang⁷², Z. Y. Wang^{1,63}, Ziyi Wang⁶³,
 D. H. Wei¹⁴, F. Weidner⁶⁸, S. P. Wen¹, Y. R. Wen³⁹, U. Wiedner³, G. Wilkinson⁶⁹, M. Wolke⁷⁵,
 L. Wollenberg³, C. Wu³⁹, J. F. Wu^{1,8}, L. H. Wu¹, L. J. Wu^{1,63}, X. Wu^{12,g}, X. H. Wu³⁴, Y. Wu^{71,58},
 Y. H. Wu⁵⁵, Y. J. Wu³¹, Z. Wu^{1,58}, L. Xia^{71,58}, X. M. Xian³⁹, B. H. Xiang^{1,63}, T. Xiang^{46,h},
 D. Xiao^{38,k,l}, G. Y. Xiao⁴², S. Y. Xiao¹, Y. L. Xiao^{12,g}, Z. J. Xiao⁴¹, C. Xie⁴², X. H. Xie^{46,h},
 Y. Xie⁵⁰, Y. G. Xie^{1,58}, Y. H. Xie⁶, Z. P. Xie^{71,58}, T. Y. Xing^{1,63}, C. F. Xu^{1,63}, C. J. Xu⁵⁹,
 G. F. Xu¹, H. Y. Xu^{66,2}, M. Xu^{71,58}, Q. J. Xu¹⁶, Q. N. Xu³⁰, W. Xu¹, W. L. Xu⁶⁶, X. P. Xu⁵⁵,
 Y. Xu⁴⁰, Y. C. Xu⁷⁷, Z. S. Xu⁶³, F. Yan^{12,g}, L. Yan^{12,g}, W. B. Yan^{71,58}, W. C. Yan⁸⁰, X. Q. Yan^{1,63},
 H. J. Yang^{51,f}, H. L. Yang³⁴, H. X. Yang¹, J. H. Yang⁴², T. Yang¹, Y. Yang^{12,g}, Y. F. Yang⁴³,
 Y. F. Yang^{1,63}, Y. X. Yang^{1,63}, Z. W. Yang^{38,k,l}, Z. P. Yao⁵⁰, M. Ye^{1,58}, M. H. Ye⁸, J. H. Yin¹,
 Junhao Yin⁴³, Z. Y. You⁵⁹, B. X. Yu^{1,58,63}, C. X. Yu⁴³, G. Yu^{1,63}, J. S. Yu^{25,i}, M. C. Yu⁴⁰,
 T. Yu⁷², X. D. Yu^{46,h}, Y. C. Yu⁸⁰, C. Z. Yuan^{1,63}, J. Yuan³⁴, J. Yuan⁴⁵, L. Yuan², S. C. Yuan^{1,63},
 Y. Yuan^{1,63}, Z. Y. Yuan⁵⁹, C. X. Yue³⁹, A. A. Zafar⁷³, F. R. Zeng⁵⁰, S. H. Zeng⁷², X. Zeng^{12,g},
 Y. Zeng^{25,i}, Y. J. Zeng^{1,63}, Y. J. Zeng⁵⁹, X. Y. Zhai³⁴, Y. C. Zhai⁵⁰, Y. H. Zhan⁵⁹, A. Q. Zhang^{1,63},
 B. L. Zhang^{1,63}, B. X. Zhang¹, D. H. Zhang⁴³, G. Y. Zhang¹⁹, H. Zhang^{71,58}, H. Zhang⁸⁰, H. C. Zhang^{1,58,63},
 H. H. Zhang⁵⁹, H. H. Zhang³⁴, H. Q. Zhang^{1,58,63}, H. R. Zhang^{71,58}, H. Y. Zhang^{1,58}, J. Zhang⁵⁹,
 J. Zhang⁸⁰, J. J. Zhang⁵², J. L. Zhang²⁰, J. Q. Zhang⁴¹, J. S. Zhang^{12,g}, J. W. Zhang^{1,58,63},
 J. X. Zhang^{38,k,l}, J. Y. Zhang¹, J. Z. Zhang^{1,63}, Jianyu Zhang⁶³, L. M. Zhang⁶¹, Lei Zhang⁴²,
 P. Zhang^{1,63}, Q. Y. Zhang³⁴, R. Y. Zhang^{38,k,l}, S. H. Zhang^{1,63}, Shulei Zhang^{25,i}, X. D. Zhang⁴⁵,
 X. M. Zhang¹, X. Y. Zhang⁴⁰, X. Y. Zhang⁵⁰, Y. Zhang¹, Y. Zhang⁷², Y. T. Zhang⁸⁰, Y. H. Zhang^{1,58},
 Y. M. Zhang³⁹, Yan Zhang^{71,58}, Z. D. Zhang¹, Z. H. Zhang¹, Z. L. Zhang³⁴, Z. Y. Zhang⁴³,
 Z. Y. Zhang⁷⁶, Z. Z. Zhang⁴⁵, G. Zhao¹, J. Y. Zhao^{1,63}, J. Z. Zhao^{1,58}, L. Zhao¹, Lei Zhao^{71,58},
 M. G. Zhao⁴³, N. Zhao⁷⁸, R. P. Zhao⁶³, S. J. Zhao⁸⁰, Y. B. Zhao^{1,58}, Y. X. Zhao^{31,63}, Z. G. Zhao^{71,58},
 A. Zhemchugov^{36,b}, B. Zheng⁷², B. M. Zheng³⁴, J. P. Zheng^{1,58}, W. J. Zheng^{1,63}, Y. H. Zheng⁶³,
 B. Zhong⁴¹, X. Zhong⁵⁹, H. Zhou⁵⁰, J. Y. Zhou³⁴, L. P. Zhou^{1,63}, S. Zhou⁶, X. Zhou⁷⁶, X. K. Zhou⁶,
 X. R. Zhou^{71,58}, X. Y. Zhou³⁹, Y. Z. Zhou^{12,g}, A. N. Zhu⁶³, J. Zhu⁴³, K. Zhu¹, K. J. Zhu^{1,58,63},

K. S. Zhu^{12,g}, L. Zhu³⁴, L. X. Zhu⁶³, S. H. Zhu⁷⁰, T. J. Zhu^{12,g}, W. D. Zhu⁴¹, Y. C. Zhu^{71,58},
Z. A. Zhu^{1,63}, J. H. Zou¹, J. Zu^{71,58}

¹ *Institute of High Energy Physics, Beijing 100049, People's Republic of China*

² *Beihang University, Beijing 100191, People's Republic of China*

³ *Bochum Ruhr-University, D-44780 Bochum, Germany*

⁴ *Budker Institute of Nuclear Physics SB RAS (BINP), Novosibirsk 630090, Russia*

⁵ *Carnegie Mellon University, Pittsburgh, Pennsylvania 15213, USA*

⁶ *Central China Normal University, Wuhan 430079, People's Republic of China*

⁷ *Central South University, Changsha 410083, People's Republic of China*

⁸ *China Center of Advanced Science and Technology, Beijing 100190, People's Republic of China*

⁹ *China University of Geosciences, Wuhan 430074, People's Republic of China*

¹⁰ *Chung-Ang University, Seoul, 06974, Republic of Korea*

¹¹ *COMSATS University Islamabad, Lahore Campus, Defence Road, Off Raiwind Road, 54000 Lahore, Pakistan*

¹² *Fudan University, Shanghai 200433, People's Republic of China*

¹³ *GSI Helmholtzcentre for Heavy Ion Research GmbH, D-64291 Darmstadt, Germany*

¹⁴ *Guangxi Normal University, Guilin 541004, People's Republic of China*

¹⁵ *Guangxi University, Nanning 530004, People's Republic of China*

¹⁶ *Hangzhou Normal University, Hangzhou 310036, People's Republic of China*

¹⁷ *Hebei University, Baoding 071002, People's Republic of China*

¹⁸ *Helmholtz Institute Mainz, Staudinger Weg 18, D-55099 Mainz, Germany*

¹⁹ *Henan Normal University, Xinxiang 453007, People's Republic of China*

²⁰ *Henan University, Kaifeng 475004, People's Republic of China*

²¹ *Henan University of Science and Technology, Luoyang 471003, People's Republic of China*

²² *Henan University of Technology, Zhengzhou 450001, People's Republic of China*

²³ *Huangshan College, Huangshan 245000, People's Republic of China*

²⁴ *Hunan Normal University, Changsha 410081, People's Republic of China*

²⁵ *Hunan University, Changsha 410082, People's Republic of China*

²⁶ *Indian Institute of Technology Madras, Chennai 600036, India*

²⁷ *Indiana University, Bloomington, Indiana 47405, USA*

²⁸ *INFN Laboratori Nazionali di Frascati , (A)INFN Laboratori Nazionali di Frascati, I-00044, Frascati, Italy; (B)INFN Sezione di Perugia, I-06100, Perugia, Italy; (C)University of Perugia, I-06100, Perugia, Italy*

²⁹ *INFN Sezione di Ferrara, (A)INFN Sezione di Ferrara, I-44122, Ferrara, Italy; (B)University of Ferrara, I-44122, Ferrara, Italy*

³⁰ *Inner Mongolia University, Hohhot 010021, People's Republic of China*

³¹ *Institute of Modern Physics, Lanzhou 730000, People's Republic of China*

³² *Institute of Physics and Technology, Peace Avenue 54B, Ulaanbaatar 13330, Mongolia*

³³ *Instituto de Alta Investigación, Universidad de Tarapacá, Casilla 7D, Arica 1000000, Chile*

³⁴ *Jilin University, Changchun 130012, People's Republic of China*

³⁵ *Johannes Gutenberg University of Mainz, Johann-Joachim-Becher-Weg 45, D-55099 Mainz, Germany*

³⁶ *Joint Institute for Nuclear Research, 141980 Dubna, Moscow region, Russia*

³⁷ *Justus-Liebig-Universitaet Giessen, II. Physikalisches Institut, Heinrich-Buff-Ring 16, D-35392 Giessen, Germany*

³⁸ *Lanzhou University, Lanzhou 730000, People's Republic of China*

³⁹ *Liaoning Normal University, Dalian 116029, People's Republic of China*

⁴⁰ *Liaoning University, Shenyang 110036, People's Republic of China*

- ⁴¹ *Nanjing Normal University, Nanjing 210023, People's Republic of China*
- ⁴² *Nanjing University, Nanjing 210093, People's Republic of China*
- ⁴³ *Nankai University, Tianjin 300071, People's Republic of China*
- ⁴⁴ *National Centre for Nuclear Research, Warsaw 02-093, Poland*
- ⁴⁵ *North China Electric Power University, Beijing 102206, People's Republic of China*
- ⁴⁶ *Peking University, Beijing 100871, People's Republic of China*
- ⁴⁷ *Qufu Normal University, Qufu 273165, People's Republic of China*
- ⁴⁸ *Renmin University of China, Beijing 100872, People's Republic of China*
- ⁴⁹ *Shandong Normal University, Jinan 250014, People's Republic of China*
- ⁵⁰ *Shandong University, Jinan 250100, People's Republic of China*
- ⁵¹ *Shanghai Jiao Tong University, Shanghai 200240, People's Republic of China*
- ⁵² *Shanxi Normal University, Linfen 041004, People's Republic of China*
- ⁵³ *Shanxi University, Taiyuan 030006, People's Republic of China*
- ⁵⁴ *Sichuan University, Chengdu 610064, People's Republic of China*
- ⁵⁵ *Soochow University, Suzhou 215006, People's Republic of China*
- ⁵⁶ *South China Normal University, Guangzhou 510006, People's Republic of China*
- ⁵⁷ *Southeast University, Nanjing 211100, People's Republic of China*
- ⁵⁸ *State Key Laboratory of Particle Detection and Electronics, Beijing 100049, Hefei 230026, People's Republic of China*
- ⁵⁹ *Sun Yat-Sen University, Guangzhou 510275, People's Republic of China*
- ⁶⁰ *Suranaree University of Technology, University Avenue 111, Nakhon Ratchasima 30000, Thailand*
- ⁶¹ *Tsinghua University, Beijing 100084, People's Republic of China*
- ⁶² *Turkish Accelerator Center Particle Factory Group, (A)Istinye University, 34010, Istanbul, Turkey; (B)Near East University, Nicosia, North Cyprus, 99138, Mersin 10, Turkey*
- ⁶³ *University of Chinese Academy of Sciences, Beijing 100049, People's Republic of China*
- ⁶⁴ *University of Groningen, NL-9747 AA Groningen, The Netherlands*
- ⁶⁵ *University of Hawaii, Honolulu, Hawaii 96822, USA*
- ⁶⁶ *University of Jinan, Jinan 250022, People's Republic of China*
- ⁶⁷ *University of Manchester, Oxford Road, Manchester, M13 9PL, United Kingdom*
- ⁶⁸ *University of Muenster, Wilhelm-Klemm-Strasse 9, 48149 Muenster, Germany*
- ⁶⁹ *University of Oxford, Keble Road, Oxford OX13RH, United Kingdom*
- ⁷⁰ *University of Science and Technology Liaoning, Anshan 114051, People's Republic of China*
- ⁷¹ *University of Science and Technology of China, Hefei 230026, People's Republic of China*
- ⁷² *University of South China, Hengyang 421001, People's Republic of China*
- ⁷³ *University of the Punjab, Lahore-54590, Pakistan*
- ⁷⁴ *University of Turin and INFN, (A)University of Turin, I-10125, Turin, Italy; (B)University of Eastern Piedmont, I-15121, Alessandria, Italy; (C)INFN, I-10125, Turin, Italy*
- ⁷⁵ *Uppsala University, Box 516, SE-75120 Uppsala, Sweden*
- ⁷⁶ *Wuhan University, Wuhan 430072, People's Republic of China*
- ⁷⁷ *Yantai University, Yantai 264005, People's Republic of China*
- ⁷⁸ *Yunnan University, Kunming 650500, People's Republic of China*
- ⁷⁹ *Zhejiang University, Hangzhou 310027, People's Republic of China*
- ⁸⁰ *Zhengzhou University, Zhengzhou 450001, People's Republic of China*
- ^a *Deceased*
- ^b *Also at the Moscow Institute of Physics and Technology, Moscow 141700, Russia*
- ^c *Also at the Novosibirsk State University, Novosibirsk, 630090, Russia*
- ^d *Also at the NRC "Kurchatov Institute", PNPI, 188300, Gatchina, Russia*

- ^e Also at Goethe University Frankfurt, 60323 Frankfurt am Main, Germany
- ^f Also at Key Laboratory for Particle Physics, Astrophysics and Cosmology, Ministry of Education; Shanghai Key Laboratory for Particle Physics and Cosmology; Institute of Nuclear and Particle Physics, Shanghai 200240, People's Republic of China
- ^g Also at Key Laboratory of Nuclear Physics and Ion-beam Application (MOE) and Institute of Modern Physics, Fudan University, Shanghai 200443, People's Republic of China
- ^h Also at State Key Laboratory of Nuclear Physics and Technology, Peking University, Beijing 100871, People's Republic of China
- ⁱ Also at School of Physics and Electronics, Hunan University, Changsha 410082, China
- ^j Also at Guangdong Provincial Key Laboratory of Nuclear Science, Institute of Quantum Matter, South China Normal University, Guangzhou 510006, China
- ^k Also at MOE Frontiers Science Center for Rare Isotopes, Lanzhou University, Lanzhou 730000, People's Republic of China
- ^l Also at Lanzhou Center for Theoretical Physics, Lanzhou University, Lanzhou 730000, People's Republic of China
- ^m Also at the Department of Mathematical Sciences, IBA, Karachi 75270, Pakistan
- ⁿ Also at Ecole Polytechnique Federale de Lausanne (EPFL), CH-1015 Lausanne, Switzerland
- ^o Also at Helmholtz Institute Mainz, Staudinger Weg 18, D-55099 Mainz, Germany